Reinforcing effect of polyurea resin coating on RC members subject to low-speed and medium-speed impact

Sonoda, Yoshimi
Department of Civil Engineering, Kyushu University

Tamai, Hiroki
Department of Civil Engineering, Kyushu University

Ifuku, Tatsuya
Department of Civil Engineering, Kyushu University

Koshiishi, Masami
Nippon Koei Co.,Ltd.

出版情報：Advances in Structural Engineering. 25 (7), pp.1609-1621, 2022-03-29. SAGE Publications
バージョン：
権利関係：

Reinforcing effect of polyurea resin coating on RC members subject to low-speed and medium-speed impact

Yoshimi Sonoda, Hiroki Tamai, Tatsuya Ifuku, Masami Koshiishi

Abstract

Polyurea resin is widely used as a coating material for civil engineering structures due to their relatively high strength and elongation ability and its applications for improving the impact resistance and explosion resistance of concrete and steel structures have also been studied. However, the reinforcing effect against lower-speed impact loads has not been well studied. In this study, we investigated the load-bearing capacity of RC structural members coated with polyurea resin under repeated impact loads using a low-speed falling weight and a medium-speed flying object. The results of low-speed repeated impact test showed that there was no significant effect under the first impact, however, when the number of impacts increased, the strengthening effect of the polyurea resin was confirmed. In addition, by coating the back side of the RC slab, the remarkable effect of preventing the scattering of concrete pieces was verified in the medium-speed repeated impact test. In this study, Finite element simulations of these two types of impacts were performed, and the strengthening effect of polyurea resin was analyzed and the same tendencies as impact tests were reproduced.

1 Introduction

Polyurea resin has relatively high strength and elongation ability, as well as excellent water retention, abrasion resistance, chemical resistance, and impact resistance; thus, it is widely used as a coating material for various civil engineering structures [1]–[6]. Recently, applications for improving the impact resistance and explosion resistance of concrete and steel structures have also been studied [7]–[14].

For example, Amin et al. [7] investigated the impact response of a steel sheet coated with polyurea resin using a direct pressure pulse test and confirmed the improved impact resistance of the steel sheet due to the coating. A numerical simulation study to investigate the impact resistance of steel plate with polyurea resin coating was conducted by Samiee et al. [8], and the dynamic response of steel plates coated with polyurea resin under low-speed impact was studied by Jiang et al. [9].

As regards extant research on concrete structural members coated with polyurea resin, an experimental

study on the explosion resistance of concrete slabs reinforced on the back side with polyurea resin was performed by Ichino et al. [12]. Further, a three-point bending test and an explosion experiment were conducted on a concrete panel coated with polyurea resin and carbon fiber reinforced plastics (CFRPs) by Chen et al. [13]. They reported that concrete panels reinforced with polyurea resin have better load-bearing performance against explosive loads than panels reinforced with CFRP but are less resistant to static load. Ha et al. [14] proposed a new composite material that combines CFRP, which is a high-rigidity and high-strength material, and polyurea, which is a high-ductility material. They coated a reinforced concrete (RC) slab with the composite material, investigated the explosion resistance of the coated, and confirmed its effectiveness.

Polyurea resins are generally recognized to have a clear reinforcing effect when coated on surfaces subject to high-speed impact and explosion loads. However, the reinforcing effect against lower-speed impact loads has not been well studied. In addition, research concerning numerical simulation of RC members coated with polyurea resin under low-speed or medium-speed impact has been scarce.

In this study, we investigated the load-bearing capacity of RC structural members coated with polyurea resin using impact tests and numerical simulations. In particular, repeated impact tests of an RC cantilever beam with low-speed falling weight, and repeated impact tests of an RC slab with a medium-speed flying object were conducted, to elucidate the fracture process of RC structural members coated with polyurea resin. Furthermore, finite element (FE) simulations of these two types of impacts were performed, and the strengthening effect of polyurea resin was analyzed on the basis of the numerical analysis results.

2 Low-speed repeated impact test of RC cantilever

To examine the response to low-velocity impact loads of RC members coated with polyurea resin, a repeated weight drop impact test was conducted on RC cantilever beams.

2.1 Experiment outline

Figure 2.1 shows a schematic diagram of the test specimen. The RC cantilever beam specimen has a length of 1000 mm and a cross-sectional dimension of 600 mm × 200 mm (width × height), and D10 (SD345) is placed as the main reinforcing bar and shear reinforcing bar. The polyurea resin was applied uniformly to the upper and lower surfaces of the beam, the upper surface of the footing, and the side surfaces, with a thickness of 2 mm. Photo 2.1 shows the drop-weight impact test device. Photo 2.2 shows the shape of the weight, and Table 2.1 shows the loading conditions. The experiment was carried out by freely dropping a weight with a mass of 1000 kg from a predetermined height and repeatedly colliding with the specimen. The initial drop was performed from a height of 300 mm, after which five drops were performed at each of 50, 100, 150 and 200mm.

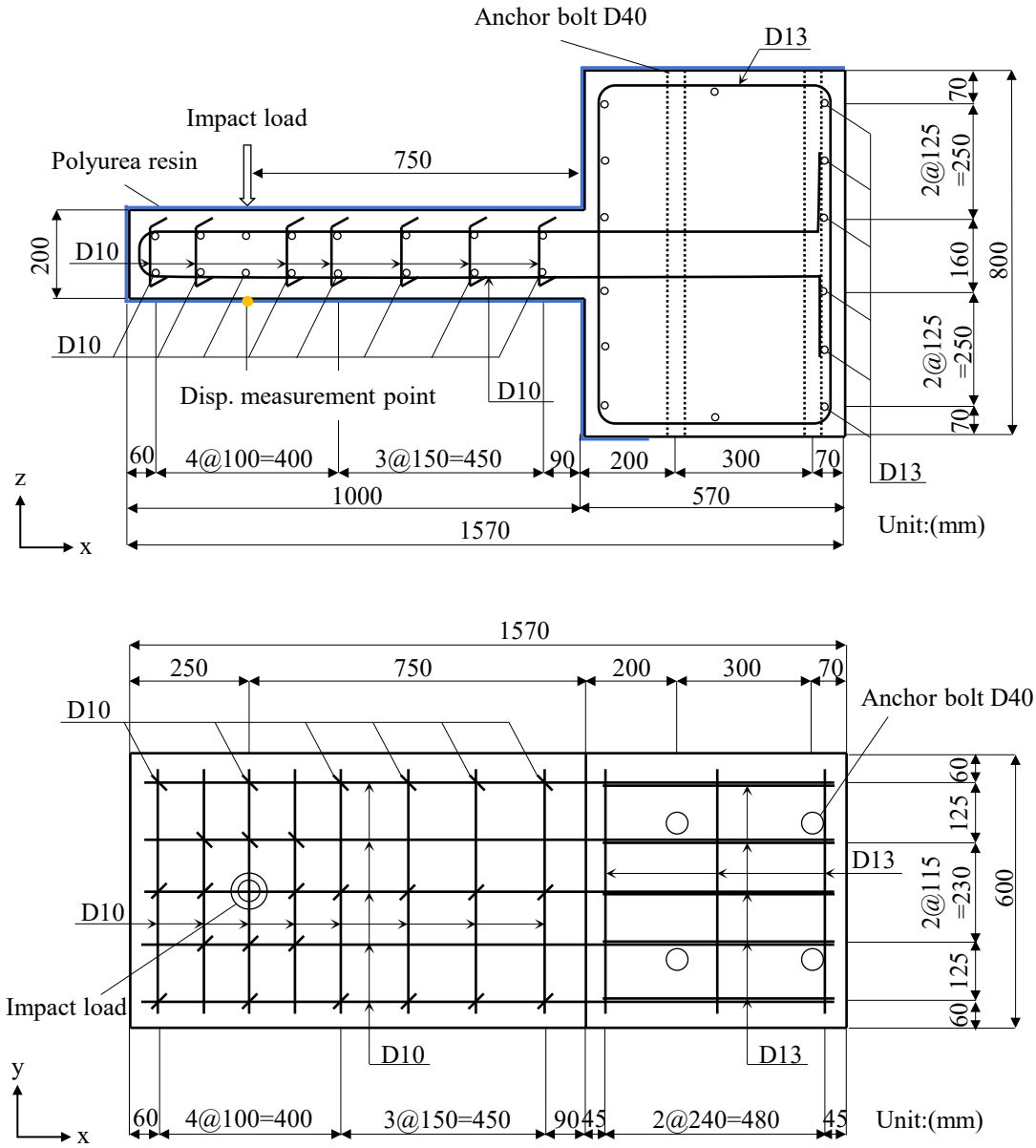

Figure 2.1 Schematic diagram of the test specimen

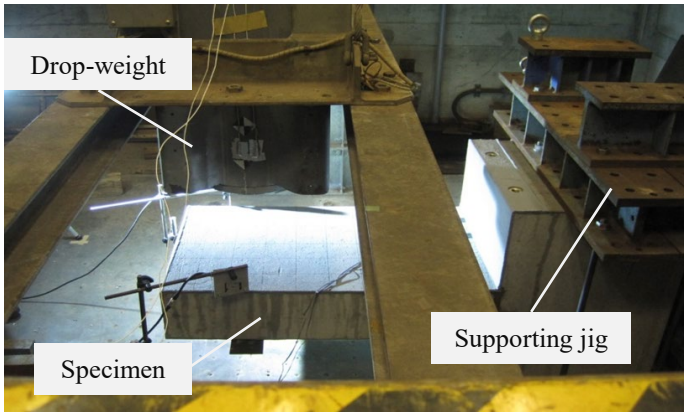

Photo 2.1 Drop-weight impact test device

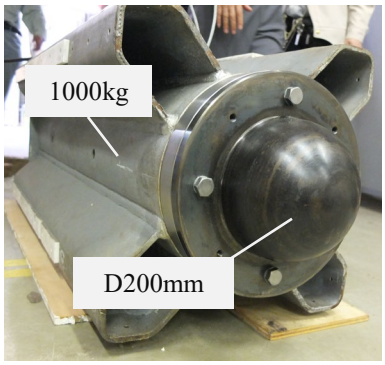

Photo-2.2 Shape of weight

Table 2.1 Loading condition

Impact Number	1	2–6	7–11	12–16	17
Drop Height (mm)	300	50	100	150	200
Impact Velocity (m/sec)	2.43	0.99	1.4	1.72	1.98

2.2 Experimental results and discussion

Figure 2.2 shows the displacement response at the first impact, and Figure 2.3 shows the relationship between the number of impacts and maximum displacement. In the first impact loading, there was almost no difference in displacement response. However, as the number of impacts increased, the displacement of the specimen coated with polyurea decreased more than that of the specimen without the coating. Furthermore, the specimen without polyurea coating collapsed as the five tension-side main reinforcing bars ruptured at the 11th impact loading. In contrast, the specimen with polyurea coating did not collapse completely until the 17th impact loading.

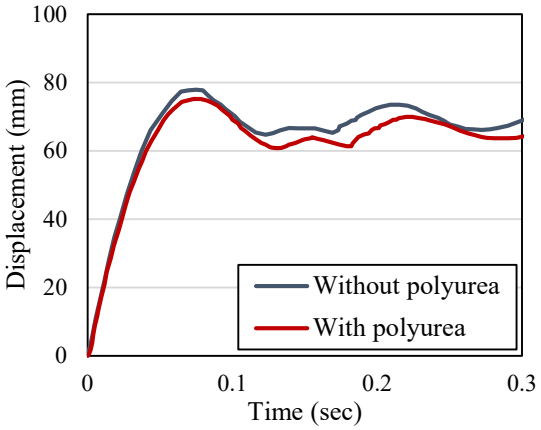

Figure 2.2 Displacement response at the first impact

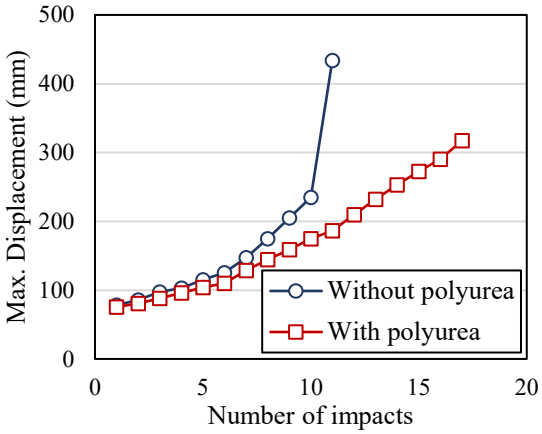

Figure 2.3 Relationship between the number of impacts and maximum displacement

(a) Specimen without polyurea coating (after 11th impact)

(b) Specimen with polyurea coating (after 17th impact)

Photo 2.3 Failure status

Photos 2.3 (a) and (b) show the state of collapse of the specimens. In the specimen without polyurea coating, large cracks occurred from the upper edge of the beam base, and the concrete on the compression side of the beam base were crushed, causing concrete pieces to peel off. Conversely, in the specimen coated with polyurea, even after the polyurea resin was peeled off at the beam base, the resin held the footing foundation and the beam member together and exerted a restoring force. It was also found that the crushed

concrete could be prevented from peeling off on the compression side of the beam base. These results confirmed that by coating with polyurea resin, the impact absorption performance can be improved by the shape-retaining effect of the polyurea resin under a low-speed repeated impact load.

3 Numerical simulations for low-speed repeated impact test of RC cantilever

3.1 Finite element model

Figure 3.1 shows the FE model for the RC cantilever. In this analysis, a half-symmetry model was used. Concrete and polyurea resin are modeled using three-dimensional solid elements, and steel bars are modeled by embedded steel truss elements.

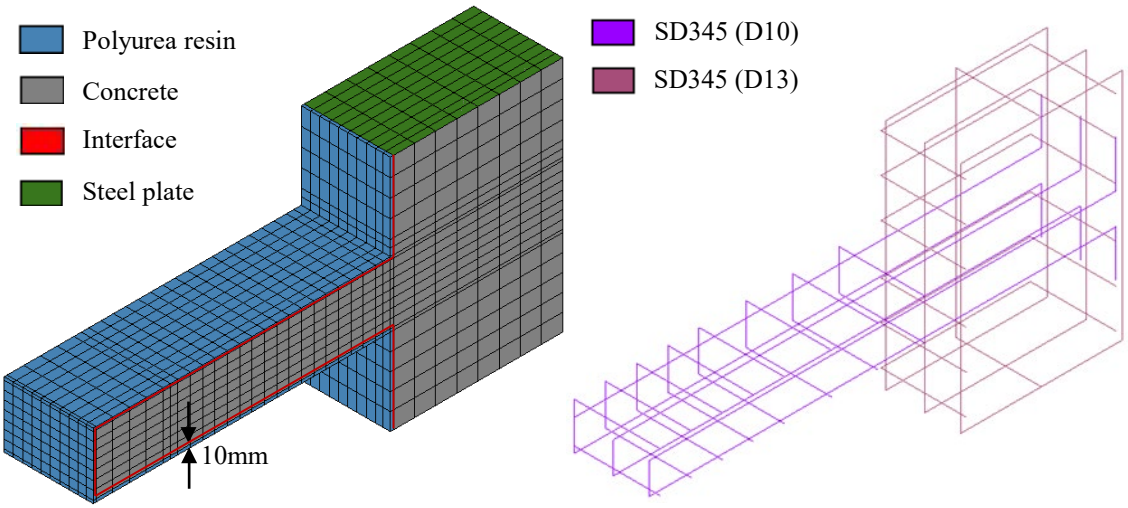

(a) RC cantilever with polyurea coating (b) Steel reinforcement

Figure 3.1 Finite element model for RC cantilever

This analysis reproduces an experiment in which the impact is repeated 10 times or more. Therefore, if the entire model is divided into fine meshes and the number of elements increases, the calculation cost will also increase. Therefore, the concrete element with a size of about 10 to 50 mm is used in this study. Along

with this, though the actual polyurea resin is coated on the beam with a thickness of 2 mm, in the analysis model, it is modeled with a thickness of 10 mm so that the aspect ratio of the polyurea resin element does not become large. In addition, to avoid overestimating stiffness at five times the actual element thickness, we used corrected Young's modulus which is divided by the rate of increase in thickness.

3.2 Physical properties

Table 3.1 shows the physical properties of each material. The values obtained by the material tests are mainly used. The Young's modulus and density of the polyurea resin are also given after the reduction described in the previous section. The Poisson's ratio of the polyurea resin follows that of Parniani et al. [15].

A rotationally distributed cracking model was used for the concrete. Figure 3.2 shows the assumed stress-strain relationship. For the compression side, a compression softening model was applied, based on the *Concrete Standard Specification* of the JSCE [16], as formulated by Equations (3.1)–(3.4).

$$\sigma_c = E_0 K(\varepsilon - \varepsilon_p) \tag{3.1}$$

$$E_0 = 2f'_{ck}/\varepsilon_c \tag{3.2}$$

$$K = exp\left\{-0.73\frac{\varepsilon}{\varepsilon_c}\left(1-\exp\left(-1.25\frac{\varepsilon}{\varepsilon_c}\right)\right)\right\} \tag{3.3}$$

$$\varepsilon_p = \varepsilon_c - 2.86\cdot\varepsilon_c\left\{1-\exp\left(-0.35\frac{\varepsilon}{\varepsilon_c}\right)\right\} \tag{3.4}$$

where σ_c is the compressive stress (N/mm²), f'_{ck} is the compressive strength (N/mm²), ε is the total strain, ε_c is the strain at compressive strength, E_0 is the initial stiffness (N/mm²), ε_p is the plastic strain, and K is the modulus of the elastic stiffness residual rate.

Table 3.1 Physical properties

Material	Mass density [kg/m³]	Young's modulus [GPa]	Poisson's ratio	Strength [MPa]
Steel	7850.8	186.5	0.3	394.1(yield), 574.5(ultimate)
Concrete	2320	29.5	0.2	25.1(compressive), 1.97(tensile)
Polyurea resin	1000 (200)	0.11 (0.02)	0.26	24.0

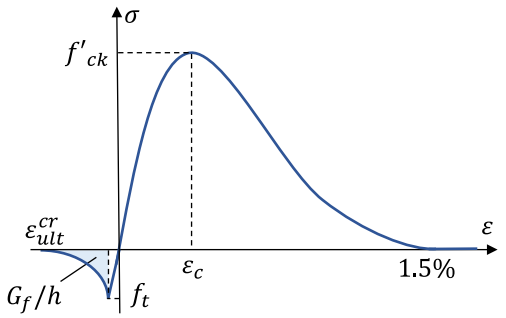

Figure 3.2 Stress-strain relationship of concrete

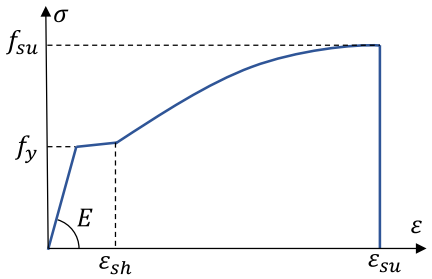

Figure 3.3 Stress-strain relationship of steel

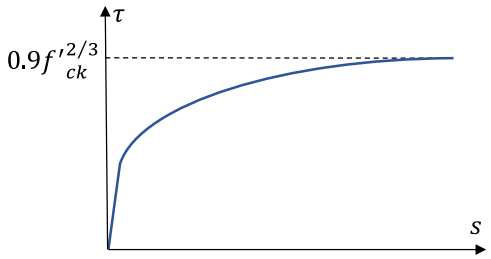

Figure 3.4 Adhesion stress-slip relationship between concrete and reinforcing bar

113

114 For the tensile side, a linear elastic material was assumed up to the tensile strength, and after the tensile
115 strength, the Hordijk model [17] given by Equations (3.5) and (3.6) was applied. The tensile strength and
116 fracture energy were calculated using Equations (3.7) and (3.8) in reference to the *Concrete Standard*
117 *Specification* of the JSCE [16].

$$\frac{\sigma^{cr}\varepsilon^{cr}}{f_t} = (1 + \left(c_1 \frac{\varepsilon^{cr}}{\varepsilon_{ult}^{cr}}\right)^3 exp\left(-c_2 \frac{\varepsilon^{cr}}{\varepsilon_{ult}^{cr}}\right) - \frac{\varepsilon^{cr}}{\varepsilon_{ult}^{cr}}(1 + c_1^3)\, exp(-c_2) \tag{3.5}$$

$$c_1 = 3, \qquad c_2 = 6.93, \qquad \varepsilon_{ult}^{cr} = 5.136\frac{G_f}{h_{cr} f_t} \tag{3.6}$$

$$f_t = 0.23 f'_{ck} \tag{3.7}$$

$$G_f = 10(d_{max})^{\frac{1}{3}} \cdot f'_{ck} \tag{3.8}$$

where σ^{cr} is the tensile stress, ε^{cr} is the cracking strain, ε_{ult}^{cr} is the ultimate cracking strain, h_{cr} is the equivalent element length (mm), f_t is the tensile strength (N/mm²), G_f is the fracture energy (N/mm), and d_{max} is the maximum size of the coarse aggregate (mm). Note that the equivalent element length h_{cr} is the value of the cubic root of the element volume.

Figure 3.3 shows the stress-strain relationship assumed for the steel material. The Dodd-Restrepo model [18] was used for the steel material model. This is a macroscopic model that predicts the cyclic stress-strain behavior of reinforcing bars, and it can take into account both the Bauschinger effect and the fracture behavior due to the reduction of stress when the fracture strain is reached. In Figure 3.3, f_y is the yield strength (N/mm²), ε_{sh} is the strain at the beginning of hardening, f_{su} is the rupture strength (N/mm²), and ε_{su} is the rupture strain.

The interface element at the interface between the concrete and the reinforcing bar introduces the adhesion stress-slip relationship proposed by Shima et al. [19], which is shown in Figure 3.4 and Equation (3.9). Note that linear elasticity is assumed in the normal direction of the interface element.

$$\tau = 0.9 \times {f'_{ck}}^{2/3}\left(1 - e^{-40\left(\frac{s}{D}\right)^{0.6}}\right) \tag{3.9}$$

where τ is the adhesion stress (N/mm²), s is the slip (mm), and D is the bar diameter (mm).

To investigate the material properties of polyurea resin, uniaxial tensile tests were conducted at a tensile speed of 50 mm/min using the dumbbell test specimen shown in Figure 3.5 (a). Figure 3.5 (b) shows the stress-strain relationship obtained from the uniaxial tensile tests.

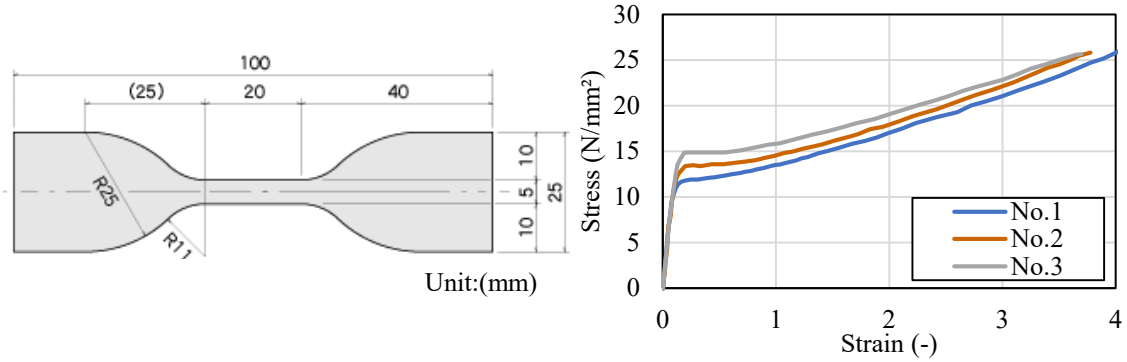

(a) Dumbbell test specimen (b) Stress-strain relationship of polyurea resin

Figure 3.5 Uniaxial tensile tests using the dumbbell test specimen

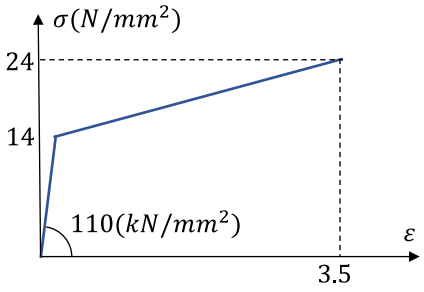

Figure 3.6 Stress-strain relationship of polyurea resin

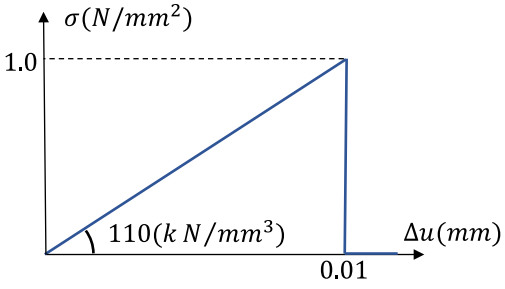

Figure 3.7 Adhesion stress-relative displacement relationship between polyurea resin and concrete

Several constitutive models have been proposed to describe the stress-strain behavior of polyurea resins. Amirkhizi et al. [20] proposed an experimentally based linear viscoelastic constitutive model that incorporated the classical Williams–Landel–Ferry (WLF) time-temperature transformation and pressure response. Li et al. [21] proposed a hyper-viscoelastic constitutive model for polyurea resin that incorporates the Ogden model and a nonlinear viscoelastic model. Zhang et al. [22] proposed a bilinear constitutive model describing the temperature, strain rate, and pressure dependence of the stress-strain behavior. However, many of the proposed constitutive models focus on the compressive characteristics of polyurea

148 resin, while a few have focused on the tensile characteristics. Furthermore, many of these constitutive
149 models are complex, which makes them difficult to apply. Therefore, the polyurea resin was assumed to be
150 a nonlinear elastoplastic material, and the stress-strain relationship shown in Figure 3.6 was assumed
151 because the focus of this study was on the tensile characteristics of the polyurea, and the basic investigation
152 of the coating effect was the objective of the analysis. Here, the unloading gradient of the polyurea resin is
153 equal to the initial stiffness, and residual strain is generated during unloading; therefore, the evaluation is
154 safer than when modeling as a hyper-elastic material.
155 An interface element is provided at the interface between the polyurea resin and the concrete, and the
156 adhesion stress-relative displacement relationship shown in Figure 3.7 is applied. Adhesion breaking was
157 expressed by setting the transfer force to zero when the stress generated in the interface element exceeded
158 the adhesion strength. Here, the initial stiffness of interface element is assumed as the stiffness of the
159 polyurea resin, which is the weaker stiffness material side, and the adhesion strength is 1.0 N/mm² based
160 on the results of the peeling test. The strain rate effect of each material was not considered, because the
161 purpose of the analysis in this study was not to reproduce the phenomenon accurately but to evaluate the
162 effect of polyurea resin coating by relative comparison.
163
164 ### 3.3 Boundary condition
165 As shown in Figure 3.8, the boundary conditions were set to be the same as those in the experiment
166 described in Section 2.1. The bottom surface of the foundation is fixed in the triaxial direction, a steel plate
167 is installed on the top surface, and only the vertical direction of the plate is fixed. An interface element is
168 created at the interface between the plate and the foundation, and the force is transmitted only in the vertical
169 direction.

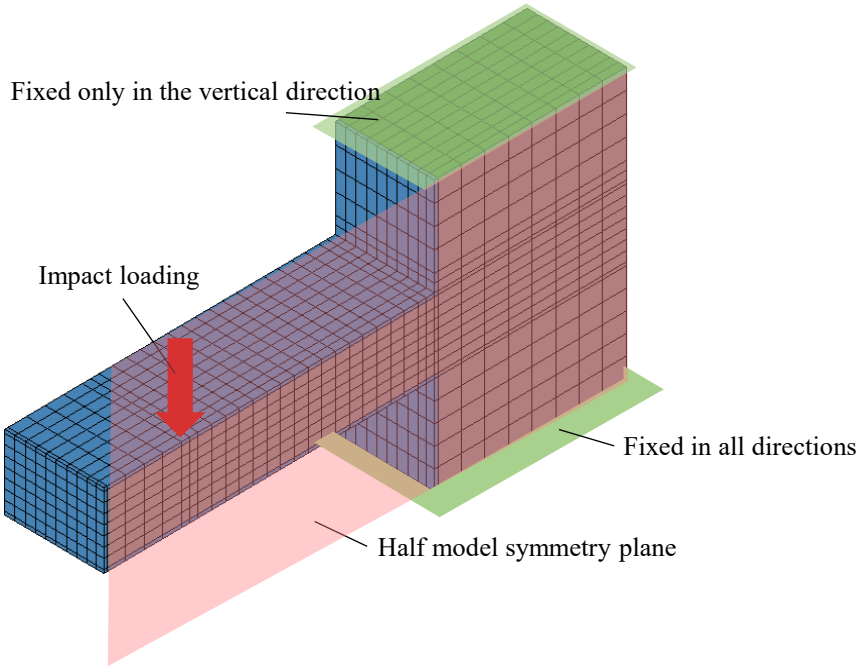

Figure 3.8 Boundary conditions

When impact analysis is conducted using finite element modeling (FEM), the impactor and the object to be impacted are modeled using finite elements, and the phenomenon is generally reproduced by solving a dynamic contact problem. However, numerical analysis of contact problems is computationally expensive, especially for the present analysis, which requires solving repeated impact loads with more than 10 impacts. Therefore, in this analysis, we adopted the method of directly inputting the impact load to the impact surface of the object to be impacted. Figure 3.9 shows the actual impact load input in the repeated impact analysis.

First, the input load for the first impact was created by approximating the impact force waveform obtained from the experiment with a figure consisting of an isosceles triangle and a rectangle. Next, the input load waveform for the second and subsequent impacts was created by assuming that the impact duration was the same as the first impact, and adjusting only the impact force so that the impulse was equal because there were no experimental results. The impulse was obtained by multiplying the change in velocity

of weight dropped freely from a given height until it stopped after impact(see Equation (3.10)). The increase in the height of the falling weight due to the residual displacement of the RC beam was added to the prescribed height. In this analysis, the number of impacts was set to 14 to carry out the analysis until the maximum displacement of the uncovered case reached the terminal displacement obtained in the experiment.

$$I = m \times (v_1 - v_0) \tag{3.10}$$

where I is the impulse received by the impacted object (kg m/s), m is the mass of the dropped weight (kg), v_0 is the velocity immediately before the impact (m/s), and v_1 is the velocity immediately after the impact (m/s).

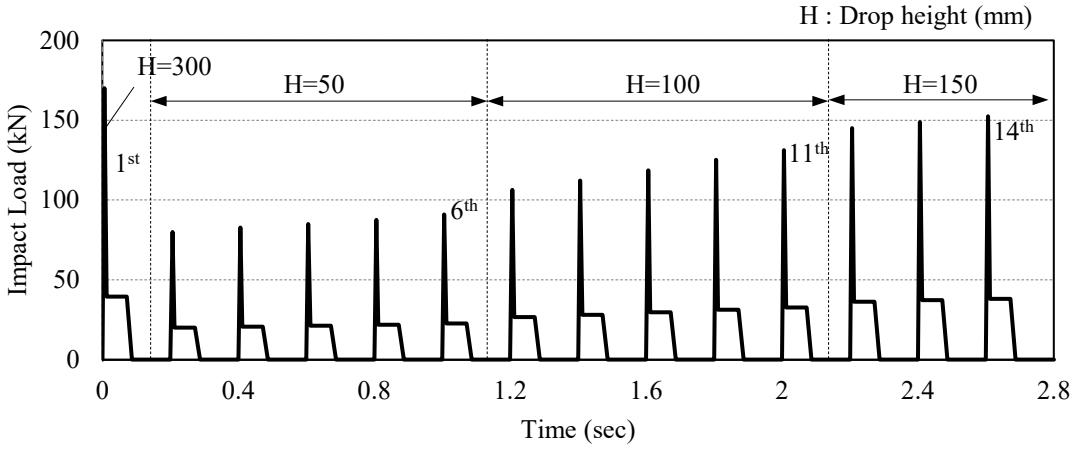

Figure 3.9 Input load waveform set for repeated impact analysis

3.4 Analysis method

The FE software DIANA 10.5 was used for this analysis. The Newmark β method (β = 0.25) was used for the time integration method. Rayleigh attenuation is assumed. Equations (3.11) and (3.12) show the equations for the Rayleigh attenuation parameters α and β, where ω_1 and ω_2 are the primary and secondary frequencies, respectively, and h_1 and h_2 are the critical attenuations (= 5%) corresponding to

each mode.

$$\beta = 2(\omega_1 h_1 - \omega_2 h_2)/\omega_1^2 - \omega_2^2 \tag{3.11}$$

$$\alpha = 2\omega_1 h_1 - \beta\omega_1^2 \tag{3.12}$$

3.5 Analysis result and discussion

3.5.1 Comparison of analytical and experimental results

Figure 3.10 shows a comparison of the experiment results and analysis results for the relationship between the number of impacts and maximum displacement. There was no significant influence of polyurea resin on the maximum displacement at the first impact; however, it was possible to reproduce the tendency of the displacement difference to increase gradually with the number of loads.

Figure 3.10 shows that the analysis value is smaller than the experimental value after the 7th impact, and this difference increases as the number of impacts increases. One of the main reasons for this is that the impact analysis does not consider the rebound of a falling weight that occurred in the impact test. In fact, the falling weight bounced with each impact test, and damage due to multiple collisions accumulated on the test piece.

Figure 3.11 shows the strain distribution of the main reinforcing bars at the time of the 12th and 14th impacts and is divided into three layers by shades of black. The darkest black color shows reinforcing bars that have reached the rupture strain, and the next darkest shade shows the reinforcing bars that have reached the yield strain. According to this figure, for the model without polyurea coating, the outermost main rebar ruptured at the 12th impact, and the second adjacent main rebar ruptured at the 14th impact. Conversely, for the model with polyurea coating, no ruptures of the main reinforcing bar were observed even at the 14th impact. According to the experiment results, five reinforcing bars of the specimen without polyurea coating ruptured and collapsed rapidly at the 11th impact in the experiment, whereas in the analysis the reinforcing bars on the outside of the specimen without polyurea coating collapsed after the 12th impact. Because of

the difference in the number of ruptured reinforcing bars and the number of impacts until the reinforcing bars ruptured, the maximum displacement of the analysis result shows a gradual increase, as shown in Figure 3.10. From these results, it was possible to reproduce the same tendency as in the experiment results; for example, the fracture can be suppressed by coating with polyurea resin, and the maximum displacement increases with the fracture of the reinforcing bar.

The green line in the Figure 3.10 shows the displacement at the loading point when the main reinforcing bar reaches the rupturing strain under the static load condition on the cantilever. In both the impact experiment and the impact analysis, the fracture of the reinforcing bar was confirmed when the displacement exceeded the level of the green line in the figure. The displacement of the specimen with polyurea coating was below this level even at the 15th impact, and thus the reinforcing bar was considered not to have ruptured yet. Therefore, results show that the coating effect of polyurea resin can increase the number of impacts until the rupturing of the reinforcing bar by approximately five.

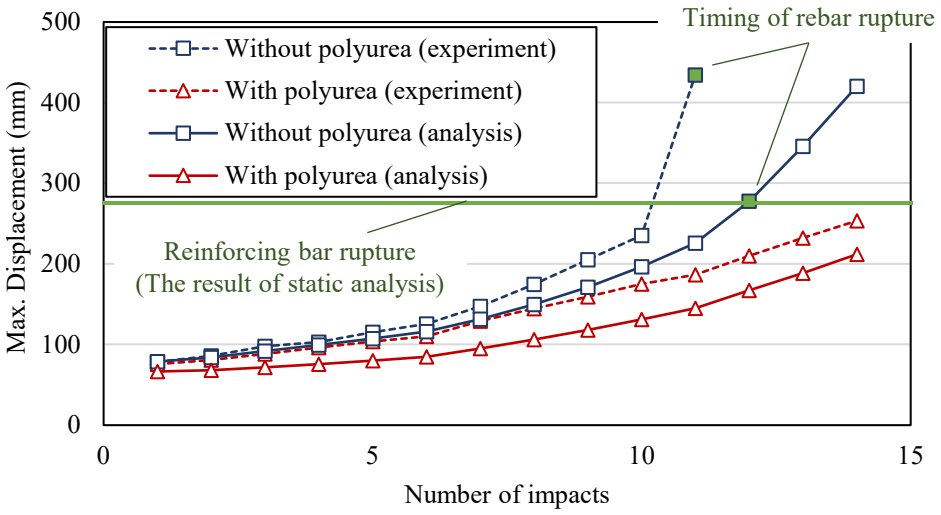

Figure 3.10 Comparison of the experiment results and analysis results for the relationship between number of loads and maximum displacement

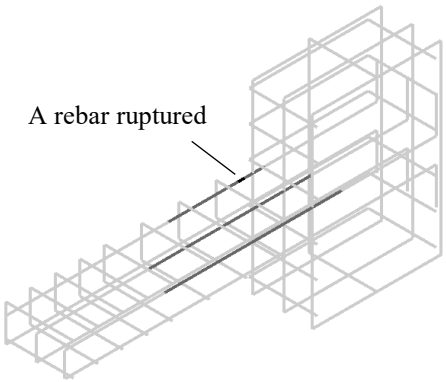

(a) Without polyurea coating (12 times)

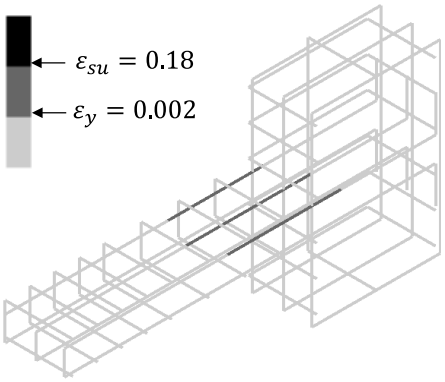

(b) With polyurea coating (12 times)

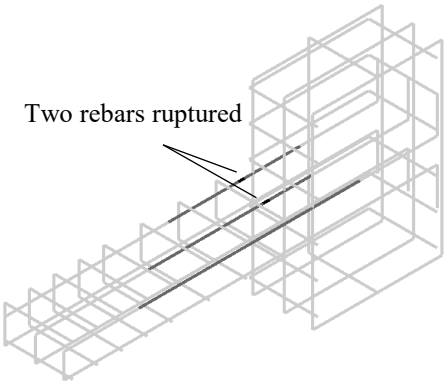

(c) Without polyurea coating (14 times)

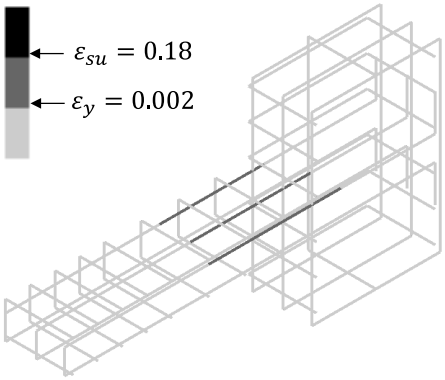

(d) With polyurea coating (14 times)

Figure 3.11 Strain distribution of the main reinforcing bars

3.5.2 Damage condition of polyurea resin

Figure 3.12 shows the equivalent stress distribution of the polyurea resin at the 14th impact. The tensile stress is particularly concentrated on the polyurea resin at the fixed end of the cantilever beam. Figure 3.13 shows the maximum principal strain distribution of the polyurea resin at the 14th impact. From this figure, it can be seen that the polyurea resin has approximately 30% strain, and there is still a margin in its elongation performance. Therefore, it is confirmed that the proposed analysis shows the same tendency as in the experiment, that the polyurea resin prevents tensile failure at the fixed end of the cantilever.

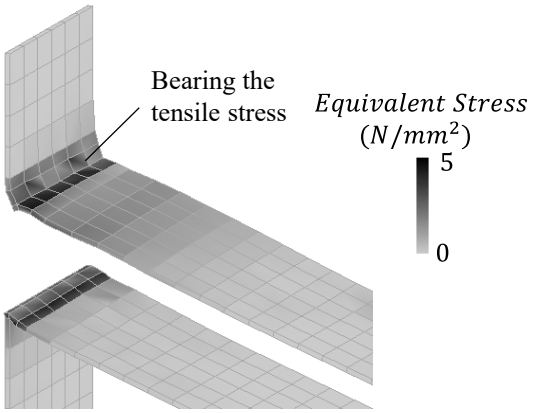

Figure 3.12 Equivalent stress distribution of the polyurea resin at the 14th impact

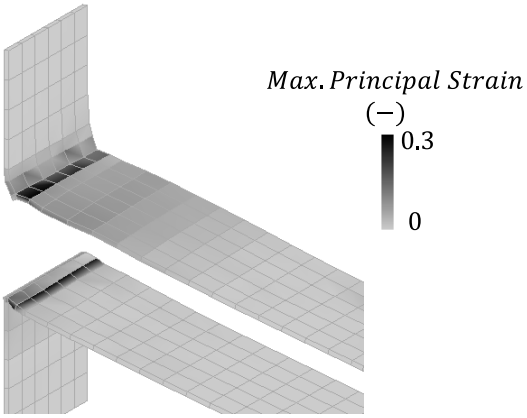

Figure 3.13 Maximum principal strain distribution of the polyurea resin at the 14th impact.

4 Push-off test and FEM analysis of polyurea resin

4.1 Test outline

To evaluate the performance of polyurea resin at preventing peeling off, a test was conducted according to the JSCE standard (JSCE-K 533-2010) and tried to reproduce the test using FEM analysis. The test was carried out by three specimens of a rectangular (400×600×60 mm) concrete member, as shown in Figure 4.1. Each specimen was cored to a depth of 55 mm in a circular shape with a diameter of 100 mm, and the back was coated with polyurea resin to a thickness of 1.5 mm. In the tests, the core was first loaded until the core (remaining concrete with a thickness of 5 mm) failed, and then loaded under displacement control up to a maximum displacement of 50 mm. At displacement points of 10, 20, and 30 mm, the range of resin peeling was marked, and the ability of the polyurea resin layer to prevent peeling was confirmed.

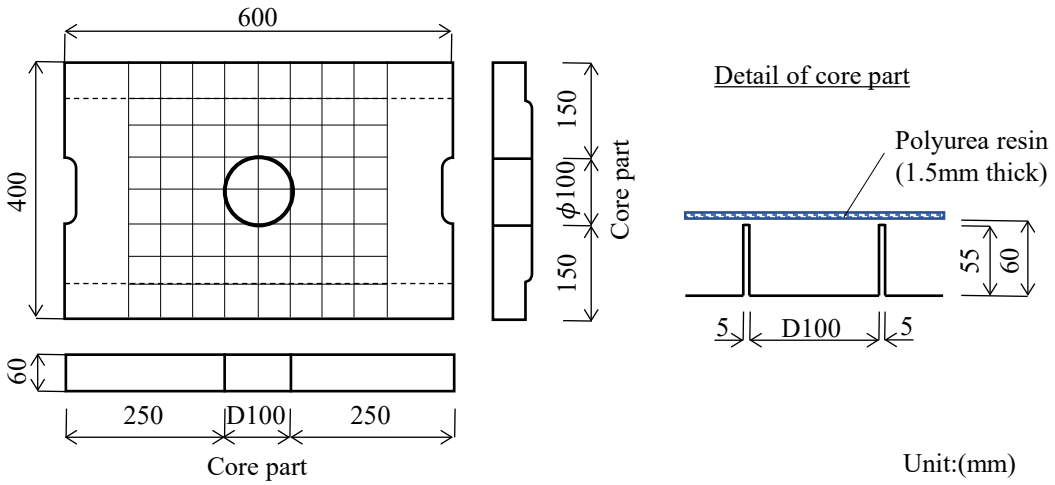

Figure 4.1 Schematic diagram of the test specimen

Figure 4.2 shows the load-displacement relationship. The range highlighted in yellow, which indicates a push-off displacement of more than 10 mm and a push-off resistance force of more than 1.5 kN, is the acceptance range defined by the standards for verification of peeling prevention performance of the 3 Japanese highway companies (East, Central and West Nippon Expressway Company Limited). From this

figure, it was confirmed that the average of the maximum loads was 2.3kN, which was within the acceptable displacement range and exhibited sufficient performance to prevent peeling. The condition after the test is shown in Photo 4.1 (a), (b), and (c). The circular lines in the photos indicate the range of polyurea resin peeling off at 10, 20, 30, and 50mm displacement, respectively. The peeling area expands as the push-off displacement increases, while the polyurea resin peels off from the concrete matrix and functions as a film covering the back surface. Figure 4.3 shows a schematic diagram showing the expansion of the peeling area by pushing out.

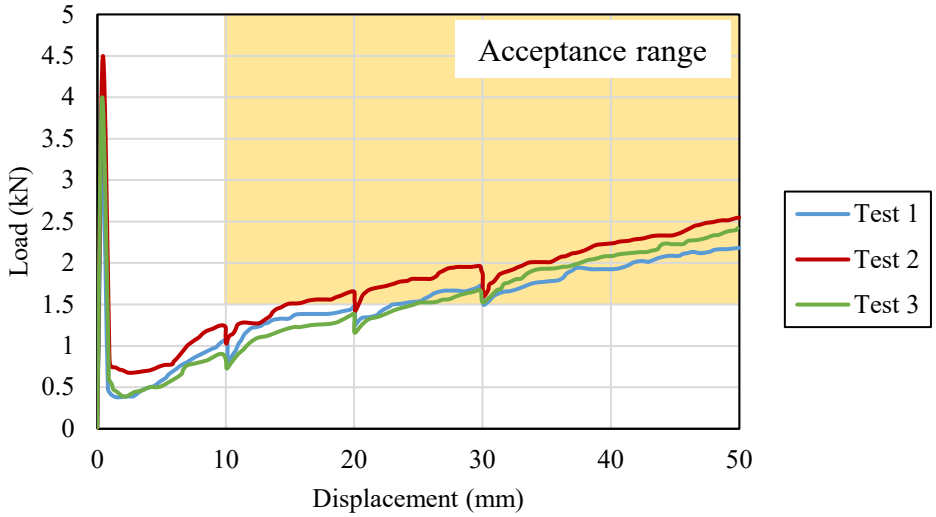

Figure 4.2 Load-displacement relationship

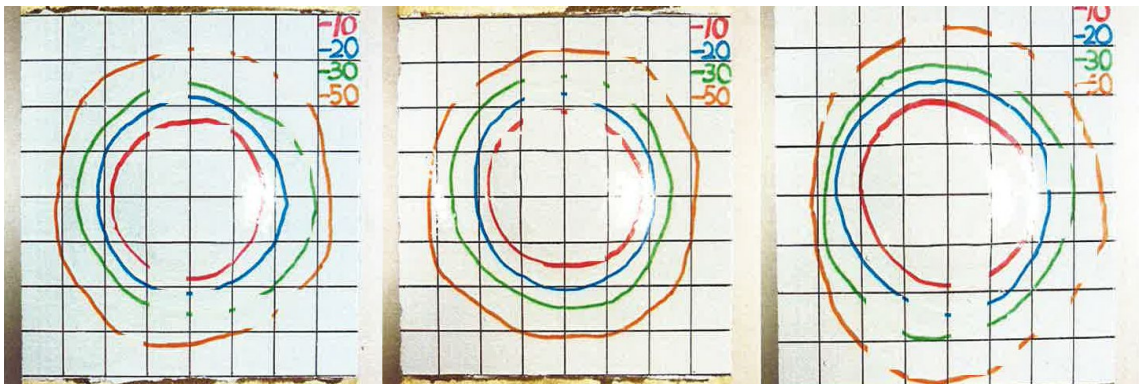

(a) Test 1 (b) Test 2 (c) Test 3

Photo 4.1 Condition of the specimens after the test

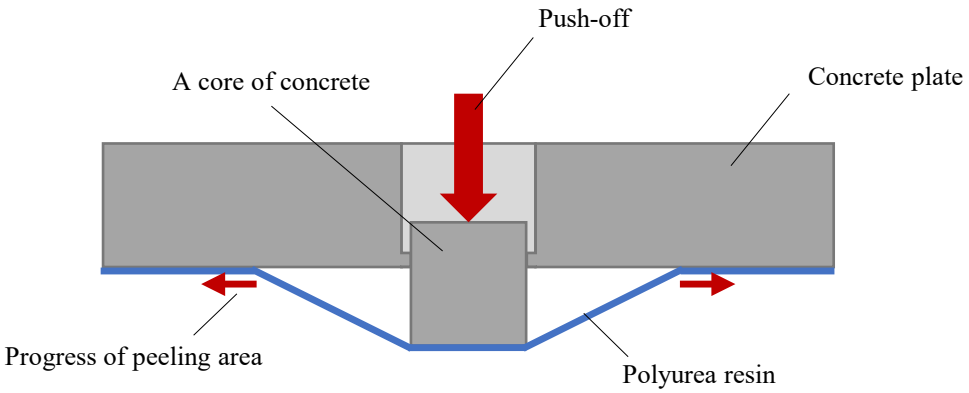

Figure 4.3 Schematic diagram showing the expansion of the peeling area

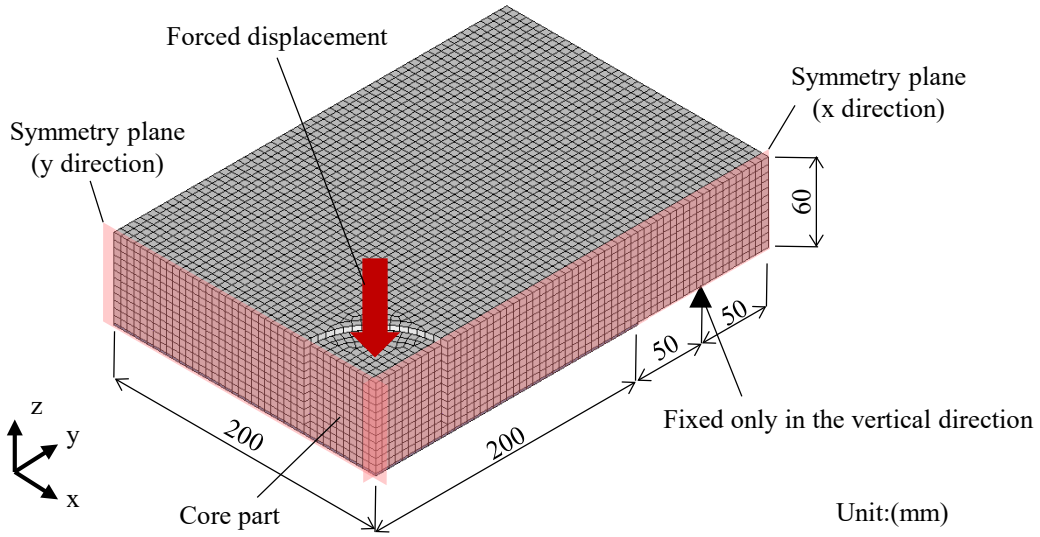

Figure 4.4 1/4 Finite element model for concrete plate

Table 4.1 Physical properties

Material	Mass density [kg/m³]	Young's modulus [kN/mm²]	Poisson's ratio	Strength [N/mm²]
Steel	7853	206	0.3	394.1(yield)
Concrete	2160	18.63	0.19	36.0(compressive), 3.6(tensile)
Polyurea resin	1000	0.11	0.26	24.0

4.2 FEM analysis result

Figure 4.4 shows the 1/4 FE model. The failure of the remaining 5 mm concrete layer in the central core is not considered in this analysis. The physical properties of each material are shown in Table 4.1. Figure 4.5 shows a comparison between the test and analysis based on the load-displacement relationship. Because the failure of the concrete at the core joint was not considered, the analysis did not show a sudden increase in the initial load condition; however, results after that were mostly able to reproduce the test.

Figure 4.6 shows the relative displacement contours in the normal direction of the interface element located between the polyurea resin and the concrete. The lower limit of the contour is set to the relative displacement at the time of adhesion failure, and the area contoured in colors other than purple indicates the area where the polyurea resin has peeled off. The model is able to reproduce the gradual expansion of the peeling area as the pushing displacement increases. Table 4.2 shows the comparison of the radius r (mm) of the peeling area between the test and analysis. The radius r of the peeling area in the test was measured from Photo 4.1 (a), (b), and (c), and averaged over all three specimens. Comparing the results of the test and the analysis, the radius of the peeling area was nearly identical.

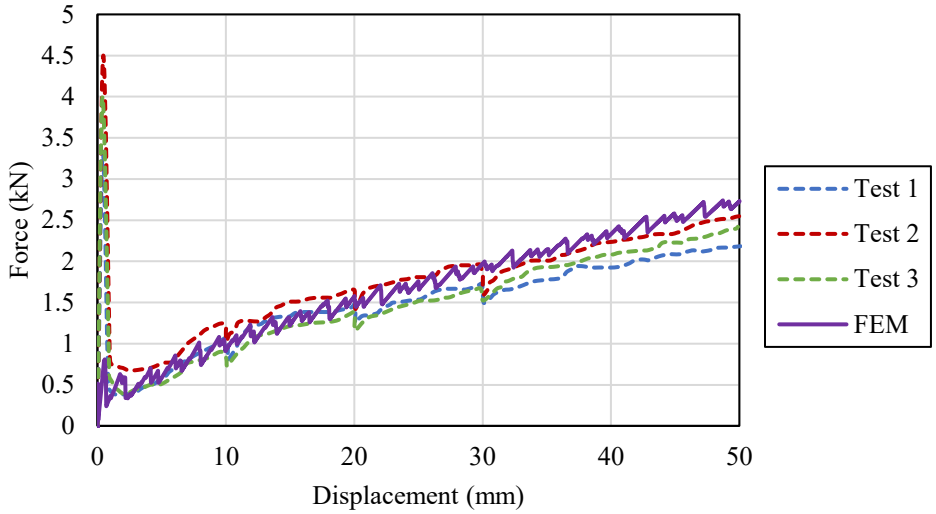

Figure 4.5 Load-displacement relationship

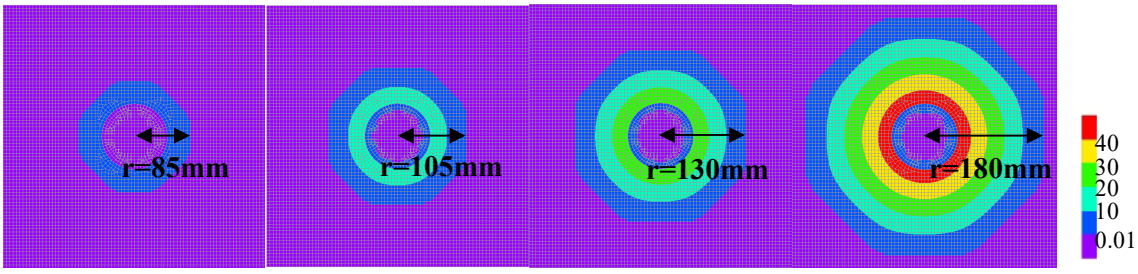

(a) Disp. 10 mm (b) Disp. 20 mm (c) Disp. 30 mm (d) Disp. 50 mm

Figure 4.6 Relative displacement contours in the normal direction

Table 4.2 Comparison of radius of peeling area between test and analysis

Displacement (mm)	Radius of peeling area : r (mm)				
	Test 1	Test 2	Test 3	**Average**	**FEM**
10	80	80	90	**83**	**85**
20	115	110	115	**113**	**105**
30	125	125	145	**132**	**130**
50	160	160	175	**165**	**180**

5 Medium-speed repeated impact of RC slab

To examine the response of RC members coated on the back side with polyurea resin to medium-velocity impact loads, a repeated lateral impact test was conducted on the RC slab.

5.1 Experiment outline

Figure 5.1 shows a schematic diagram of the test specimen. The test specimen is a square plate with dimensions of 600 mm (length)×600 mm (width) ×90 mm (height). D6(SD295A) reinforcing bars were used for the tensile side, with five bars in each direction at 125 mm intervals. A 2 mm thickness of polyurea resin was applied to the back of the specimen. The tests were conducted using a horizontal impact testing machine. Figure 5.2 shows the flying object, Photo 5.1 shows the horizontal impact test device, and Photo 5.2 shows the supporting condition. A flying object with a diameter of 50 mm, a mass of 3 kg, and repeatedly loaded at a constant speed of 10 m/sec on a test specimen supported on two sides between the upper and lower fulcrums.

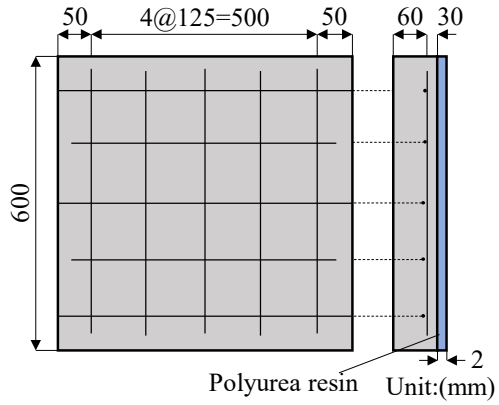

Figure 5.1 Schematic diagram of the test specimen

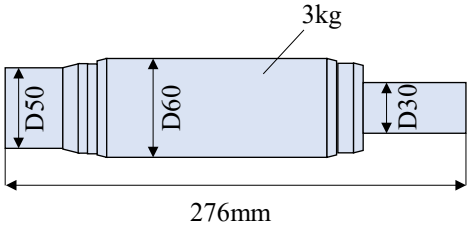

Figure 5.2 Shape of the flying object

297

Photo 5.1 Horizontal impact test device

Photo 5.2 Supporting condition

298

299 A high-speed video camera with a resolution of 260,000 pixels (512×512) and a recording speed of
300 10,000 frames per second was used, and the time history of the displacement of the flying object was
301 calculated by analyzing the obtained continuous images. Velocity and acceleration were calculated by
302 differentiating the time history of the displacement. The impact load was calculated indirectly by
303 multiplying this acceleration by the mass of the flying object.

304

305 ## 5.2 Experimental result

306 Table 5.1 shows the failure status of the front and back sides of the specimens after the final loading.

It was determined that the specimen without polyurea failed at the 5th loading when the concrete corresponding to the covering thickness of the reinforcing bar peeled off from the back side. For the specimen with polyurea coating, back side peeling occurred at the 6th loading, however the polyurea resin prevented the concrete pieces from scattering, and the test was terminated at the 13th loading. The failure mode of the test specimen was penetration from front side and slight cracking of the polyurea resin. Thus, by coating the polyurea resin on the back side, the effect of preventing the concrete pieces from scattering was confirmed.

Table 5.1 Failure status of the front and back sides of the specimens

Case	**RC slab**		**RC slab with polyurea resin on the back surface**	
	Front side	Back side	Front side	Back side
Pictures				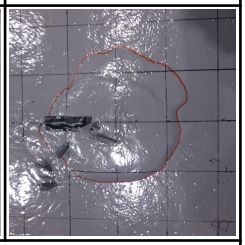
Fracture form	Back side peeling of concrete pieces		Penetration fracture of front concrete & crack fracture of polyurea	
Number of impacts	5		13	
Peeling area on back side	75000mm²		87500mm²	

Figures-5.3 (a) and (b) show the impact loads at the 1st and 5th loads, which were measured by analyzing the images captured by the high-speed video camera. Figure 5.4 shows the relationship between the maximum impact force and the number of impacts. In Figure 5.4, when comparing the maximum impact force at the 1st and 5th impacts, the specimen without polyurea showed a significant decrease at the 5th impact, which was approximately 55% less than the 1st impact due to the back side peeling which reduced

the stiffness of the member. In contrast, the maximum impact force of the specimen with polyurea coating decreased by 34% at the 5th impact and 43% at the 6th impact. These results show that the back side coating of polyurea resin not only prevented the scattering of concrete pieces that peeled off the back side, but also suppressed the reduction in stiffness when the back side peeled off.

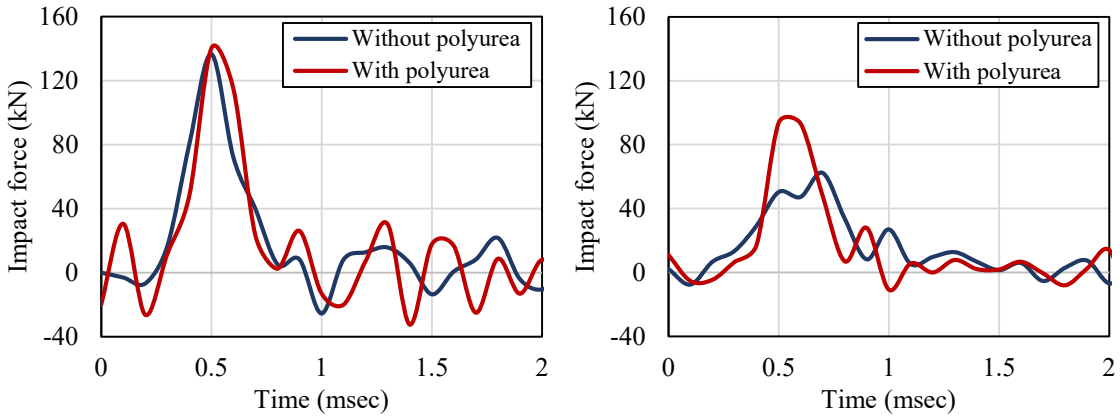

(a) 1st impact (b) 5th impact

Figure 5.3 Impact loads of the flying object

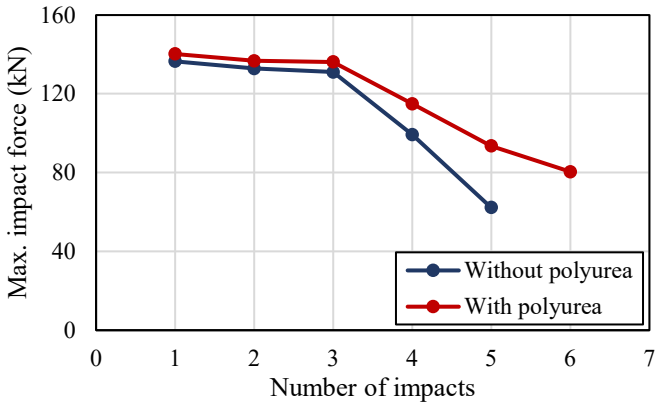

Figure 5.4 Relationship between maximum impact force and number of impacts

6 Numerical simulations for medium-speed repeated impact test of RC slab

This section numerically evaluate the effect of polyurea resin coating on the prevention of scattering and discusses the results. However, this analysis is still in the basic study stage, and the evaluation of the coating effect is limited to a relative comparison.

6.1 Finite element model and boundary condition

Figures 6.1 (a) and (b) show a schematic diagram of the model. The dimensions of the specimens were the same as the tests, and the reinforcing bars were modeled using truss elements, while the others were modeled using three-dimensional solid elements. As for the support conditions, the model was supported on two sides as shown in Figure 6.1 (b). For the loading conditions, repeated impact loading was applied by inputting the impact load. The number of loadings was the same as in the experiment. Figure 6.2 shows the impact load input for this analysis. The impact load was created by approximating the impact load wave of the flying object (Figure 5.3) as a triangular wave. In this analysis, only the concrete elements of the loading surface were assumed to be without compressive softening. Because, if the compressive failure of the loading surface element were considered, impact load would be input to the crushed element, and it would not be transferred to the entire model. To prevent this problem and impose more severe conditions on the backside peeling, the same impact load as the 4^{th} impact was input repeatedly after the 5^{th} impact.

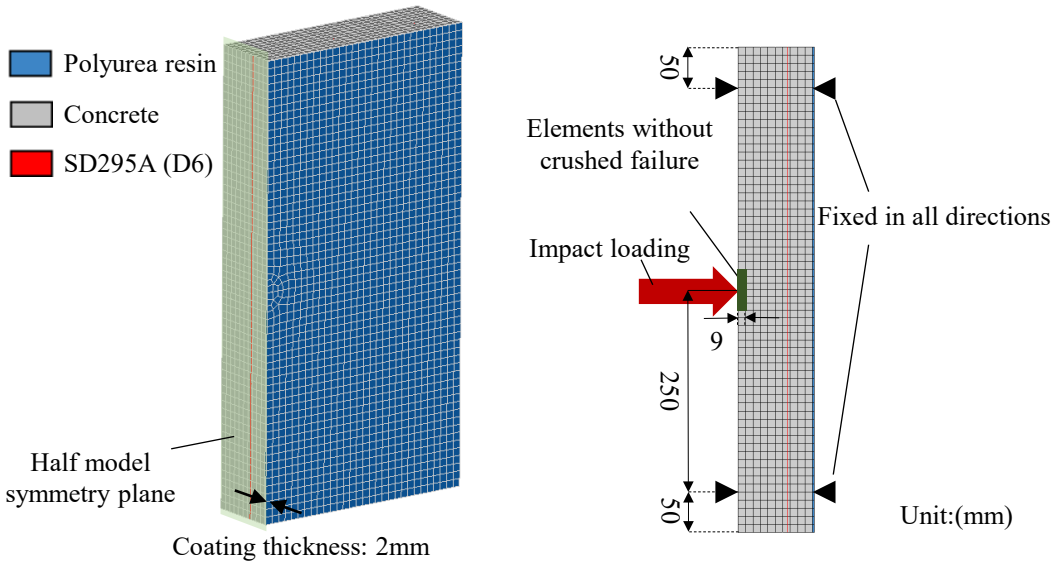

(a) 1/2 Finite Element model for RC slab (b) Boundary condition

Figure 6.1 Schematic diagram of the model

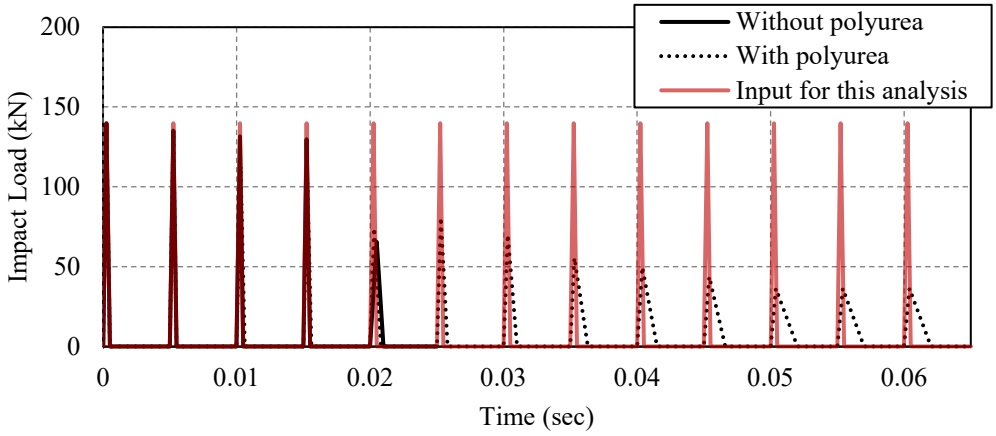

Figure 6.2 Impact load input for this analysis

6.2 Physical properties and analysis method

Table 6.2 shows the physical properties of each material. The material models for the various materials and interfaces are the same as those described in Section 3.2. and the analysis method is the same as that described in Section 3.4.

Table 6.2 Physical properties

Material	Mass density [kg/m³]	Young's modulus [kN/mm^2]	Poisson's ratio	Strength [N/mm^2]
Steel	7850	200	0.3	295(yield)
Concrete	2320	22.9	0.2	33.3(compressive), 2.38(tensile)
Polyurea resin	1000	0.11	0.26	24.0

6.3 Analysis results and discussion

Table 6.3 shows the maximum principal strain distributions for the back side of RC slabs with and without polyurea coating and the back side of polyurea resin. Comparing the strain distributions of the RC slab with and without polyurea resin coating, there is no significant difference between them. In addition, in the test, back side peeling occurred at almost the same number of impacts in both cases. Thus, it can be concluded that the back side coating of polyurea resin has almost no effect on preventing cracking and peeling of the back side. In the strain of the model without polyurea at the 5th impact shown in Table 6.3, it is assumed that back side delamination occurs as in the test. Comparing the strain distribution of the model without polyurea at the 5th impact and that of the model with polyurea at the 13th loading, it could be seen that the latter has developed more damage. However, the strain distribution on the back side of the polyurea resin showed that the maximum strain at the 13th impact was approximately 0.01, which was not far from the ultimate strain of 3.5, indicating that there was still a margin of elongation performance. In conclusion, it can be indirectly expressed that the coating of polyurea resin on the back side of the RC slab can prevent the scattering of concrete flakes even if significant damage occurs to the back side of concrete, because it is covered with sound polyurea resin (Figure 6.3).

Table 6.3 Maximum principal strain distributions for the back side of RC slabs with and without polyurea coating, and the back side of polyurea resin

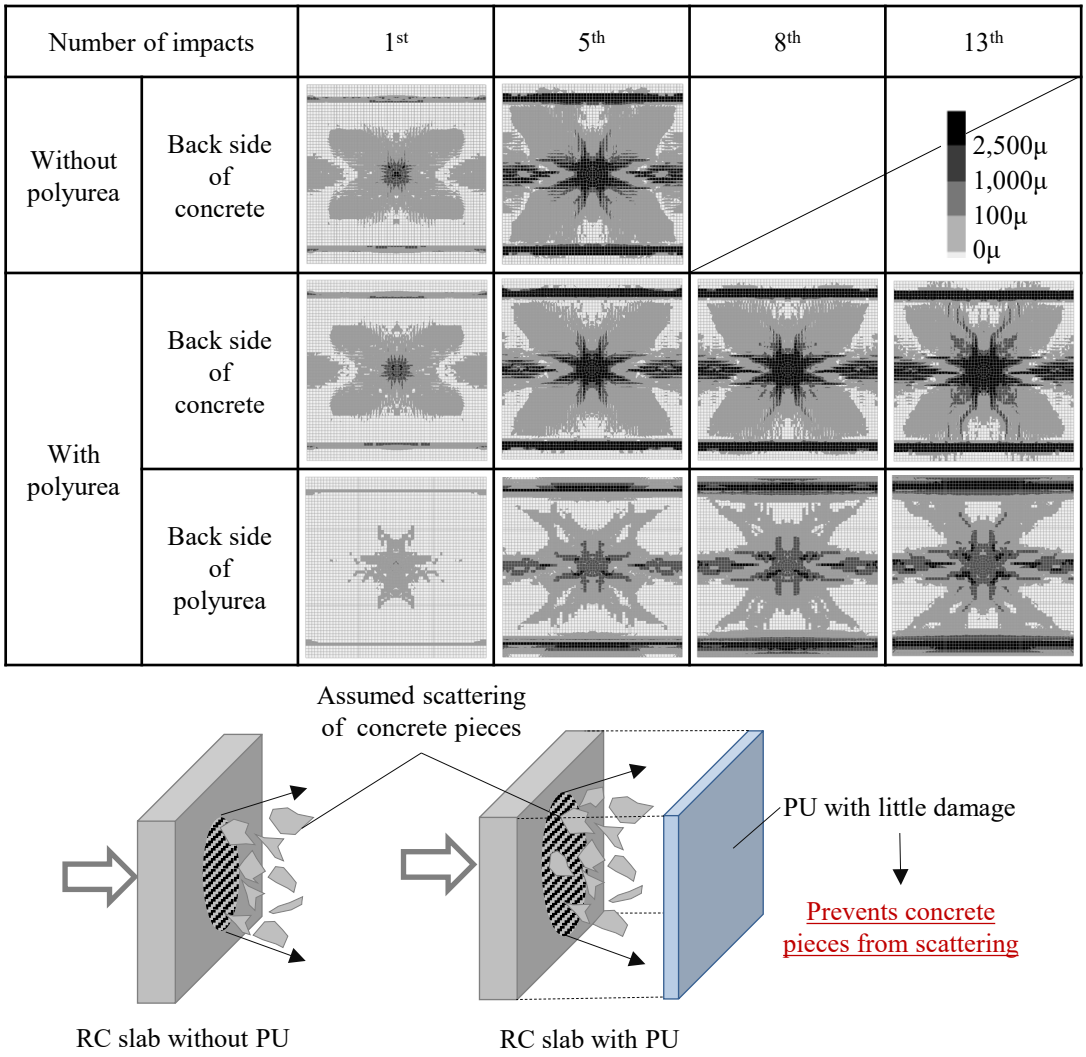

Figure 6.3 Schematic diagram of the mechanism by which polyurea resin prevents the scattering effect

364

365 ## 6.4 Effect of polyurea resin coating in case of considering penetration fracture

366 In the medium-velocity repeated collision test, it was confirmed that the resin-coated test piece had
367 penetrating fracture from front side that reached the internal reinforcing bar, but the analysis in the previous
368 section did not consider it. Therefore, it is highly possible that the load bearing performance is
369 overestimated. Therefore, we modeled penetrating fracture of the front side in FEM analysis and considered

the effect of polyurea resin on the backside peeling prevention effect.

6.4.1 Modeling penetration fracture

Figure 6.4 shows the outline of the modeling of penetrating fracture. The penetrating fracture was reproduced by sequentially deleting the concrete elements that were judged to be crushed and reducing the thickness of the RC plate. In addition, the loading surface element is deleted in layer units (when the average minimum principal strain of the in-layer element reaches 0.01) in order to keep the loading surface is flat. However, if the penetrating fracture reached to the reinforcing bar, it was assumed that the penetration would not proceed furthermore.

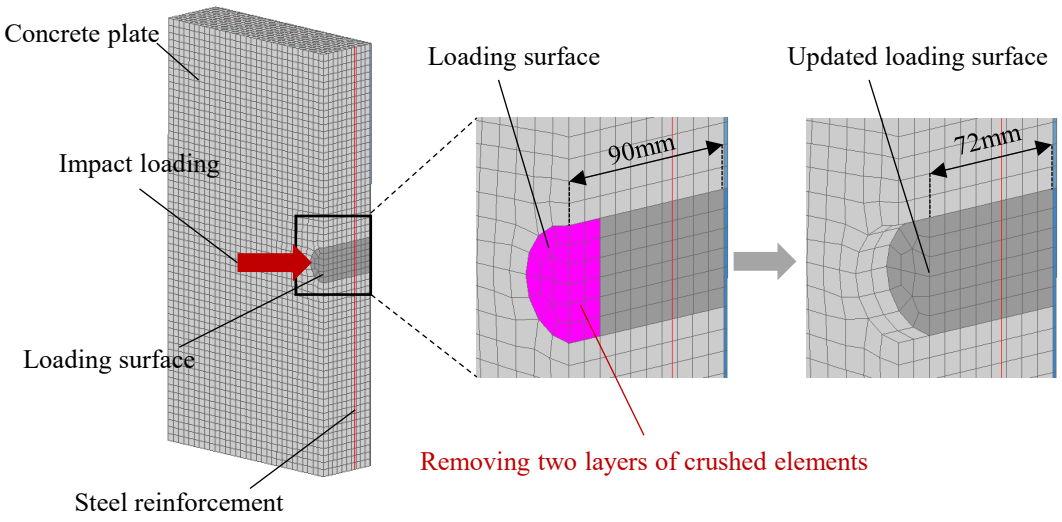

Figure 6.4 The outline of the modeling of penetrating fracture

6.4.2 Analysis result

Figure 6.5 shows the remaining thickness of the RC plate for each number of loads. From this figure, as the number of loads increased, the plate thickness decreased with the progress of penetrating fracture, and under this loading conditions, the penetration reached to the element adjacent to the reinforcing bar at the 9th shot.

384 Table 6.4 shows the maximum principal strain of the back surface of RC slab and the polyurea resin. It
385 was clearly shown that the damage was locally predominant compared to the previous results. Compared
386 to the maximum principal strain of the resin at 13th collision, the maximum strain was 0.029, which was
387 2.9 times larger than that of the maximum strain without compressive fracture assumption. Therefore, even
388 when considering the compressive fracture of concrete, the high backside peeling prevention effect of
389 polyurea resin was recognized.
390

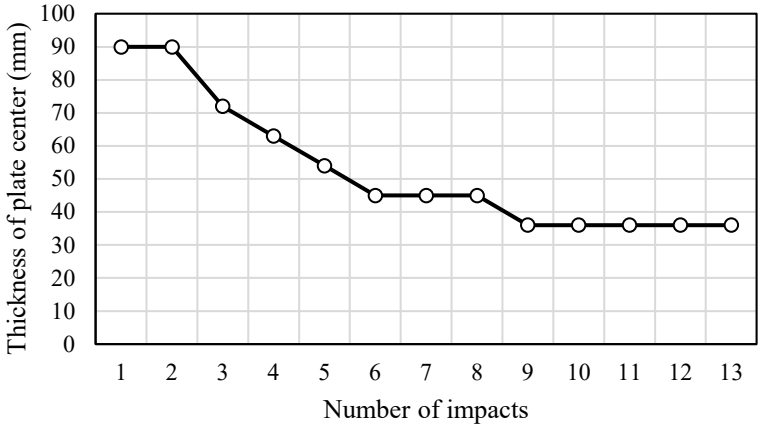

Figure 6.5 The remaining thickness of the RC plate for each number of loads

Table 6.4 Maximum principal strain distributions for the back side of RC slabs with and without polyurea coating, and the back side of polyurea resin

Number of impacts		1st	5th	8th	13th
With polyurea	Back side of concrete	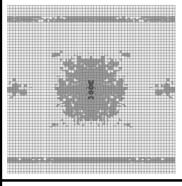	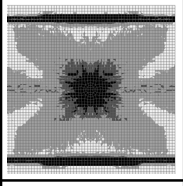	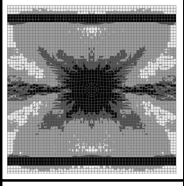	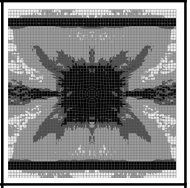
	Back side of polyurea	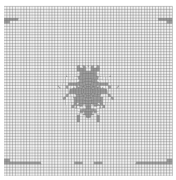	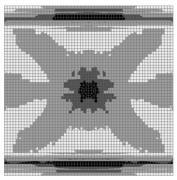	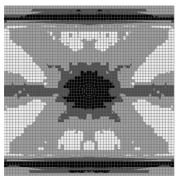	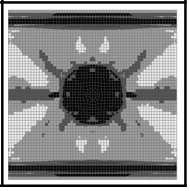

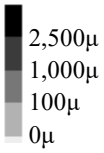

391

7 Conclusion

In this study, the impact resistance performance of RC members coated with polyurea resin under low-speed and medium-speed impact loads was examined through experiments and numerical simulations. The results of this study are summarized as follows:

1) According to the low-speed repeated impact test conducted on the RC cantilever beam, there was no significant effect under the first impact. However, when the number of impacts increased, the strengthening effect of the polyurea resin was confirmed. For example, a cross-linking effect between the upper surface of the cantilever and the pier surface of the fixed support was observed. Furthermore, the effect of preventing the concrete pieces from peeling off on the compression side of the cantilever was also confirmed. Thus, it was confirmed that the polyurea resin layer can improve the energy absorption capacity of RC structural members under impact loads.
2) When a medium-speed repeated impact test was performed on the RC slab coated with polyurea resin on the back side, it was found that the input energy required for fracture was significantly increased as compared to the case of low-speed impact. In addition, by coating the back side of the RC slab, not only the effect of preventing the scattering of concrete pieces but also the effect of suppressing the decrease in rigidity of the entire member was confirmed.
3) FE analysis of both types of impact experiments was performed, and the following effects were reproduced. The impact resistance performance of the RC beam was improved using a polyurea resin layer. In addition, although cracking and back side peeling of the concrete slab cannot be suppressed, scattering of the peeled pieces can be prevented by coating them with polyurea resin.

References

[1] Yi J, Boyce MC, Lee GF, et al. (2006)
Large deformation rate-dependent stress-strain behavior of polyurea and polyurethanes
The International Journal for the Science and Technology of Polymers 47(1): 319-329.
https://doi.org/10.1016/j.polymer.2005.10.107

[2] Roland CM, Twigg JN, Vu Y, et al. (2007)
High strain rate mechanical behavior of polyurea
The International Journal for the Science and Technology of Polymers 48(2): 574-578.
https://doi.org/10.2208/jscejmcs.72.146

[3] Sarva SS, Deschanel S, Boyce MC, et al. (2007)
Stress-strain behavior of a polyurea and a polyurethane from low to high strain rates
The International Journal for the Science and Technology of Polymers 48(8): 2208-2213.
https://doi.org/10.1016/j.polymer.2007.02.058

[4] Shim J, Mohr D (2009)
Using split Hopkinson pressure bars to perform large strain compression tests on polyurea at low, intermediate and high strain rates
International Journal of Impact Engineering 36(9): 1116-1127.
https://doi.org/10.1016/j.ijimpeng.2008.12.010

[5] Youssef G, Gupta V (2012)
Dynamic tensile strength of polyurea
Journal of Materials Research 27(02) 494-499.
https://doi.org/10.1557/jmr.2011.405

[6] Raman SN, Ngo T, Lu J, et al. (2013)
Experimental investigation on the tensile behavior of polyurea at high strain rates

Materials & Design 50: 124-129.
https://doi.org/10.1016/j.matdes.2013.02.063

[7] Amini MR, Isaacs JB, Nemat-Nasser S (2010)
Experimental investigation of response of monolithic and bilayer plates to impulsive loads
International Journal of Impact Engineering 37(1): 82-89
https://doi.org/10.1016/j.ijimpeng.2009.04.002

[8] Samiee A, Amirkhizi AV, Nemat-Nasser S (2013)
Numerical study of the effect of polyurea on the performance of steel plates under blast loads
Mechanics of Material 64: 1-10.
https://doi.org/10.1016/j.mechmat.2013.03.008

[9] Jiang Y, Zhang B, Wei J, et al. (2019)
Study on the impact resistance of polyurea-steel composite plates to low velocity impact
International Journal of Impact Engineering 133: 103357.
https://doi.org/10.1016/j.ijimpeng.2019.103357

[10] McShane GJ, Stewart C, Aronson MT, et al. (2008)
Dynamic rupture of polymer–metal bilayer plates
International Journal of Solids and Structures 45: 4407-4426.
https://doi.org/10.1016/j.ijsolstr.2008.03.017

[11] Takeuchi K, Kamiya T, Nomura T, et al. (2015)
Experimental study on the impact resistance of steel box coated with polyurea resin
Journal of Structural Engineering A 61: 851-858.

[12] Ichino H, Nagata M, Beppu M, et al. (2016)
Effects of Reinforcing Back Surface of Concrete Plates on Local Damage Caused by Explosive load

Journal of Japan Society of Civil Engineers, Ser. E2 (Materials and Concrete Structures) 72(2): 146-164.

[13] Chen Y, Wang B, Zhang B, et al. (2020)
Polyurea coating for foamed concrete panel: an efficient way to resist explosion
Defence Technology 16: 136-149.
https://doi.org/10.1016/j.dt.2019.06.010

[14] Ha JH, Yi NH, Choi JK, et al. (2011)
Experimental study on hybrid CERP-PU strengthening effect on RC panels under blast loading
Composite Structures 93: 2070-2082.
https://doi.org/10.1016/j.compstruct.2011.02.014

[15] Parniani S., Toutanji H. (2015)
Monotonic and fatigue performance of RC beams strengthened with a polyurea coating system
Construction and Building Materials 101: 22-29.
https://doi.org/10.1016/j.conbuildmat.2015.10.020

[16] Japan Society of Civil Engineering (2012)
Standard Specifications for Concrete Structures-2012, Structural Performance Evaluation
Japan Society of Civil Engineering: Tokyo, Japan,

[17] Hordijk DA (1991)
Local Approach to Fatigue of Concrete
PhD thesis, Delft University of Technology, Netherlands

[18] Dodd LL, Restrepo-Posada JI. (1995)
Model for Predicting Cyclic Behavior of Reinforcing Steel
Journal of Structural Engineering 121(3): 433–445.

[19] Shima H., Chou, LL., Okamura H. (1987)

Micro and Macro Models for Bond in Reinforced Concrete

Journal of the Faculty of Engineering, The University of Tokyo (B) 39(22): 133–194.

[20] Amirkhizi AV, Isaacs J, McGee J, et al. (2006)

An experimentally-based viscoelastic constitutive model for polyurea, including pressure and temperature effects

Philosophical Magazine 86(36): 5847-5866.

https://doi.org/10.1080/14786430600833198

[21] Li C, Lua J (2009)

A hyper-viscoelastic constitutive model for polyurea

Materials Letter 63(11): 877-880.

https://doi.org/10.1016/j.matlet.2009.01.055

[22] Zhang X, Wang J, Guo W, et al. (2017)

A bilinear constitutive response for polyureas as a function of temperature, strain rate and pressure

Journal of Applied Polymer Science 134(35): 45256

https://doi.org/10.1002/app.45256